HHS Public Access

Author manuscript

IEEE Trans Med Imaging. Author manuscript; available in PMC 2018 December 01.

Published in final edited form as:

IEEE Trans Med Imaging. 2017 December ; 36(12): 2457–2465. doi:10.1109/TMI.2017.2751679.

Hybrid Pre-log and Post-log Image Reconstruction for Computed Tomography

Guobao Wang,
Department of Biomedical Engineering, University of California - Davis, CA 95616 USA

Jian Zhou,
Toshiba Medical Research Institute USA

Zhou Yu,
Toshiba Medical Research Institute USA

Wenli Wang, and
Toshiba Medical Research Institute USA

Jinyi Qi
Department of Biomedical Engineering, University of California, Davis, CA 95616 USA

Abstract

Tomographic image reconstruction for low-dose CT is increasingly challenging as dose continues to reduce in clinical applications. Pre-log domain methods and post-log domain methods have been proposed individually and each method has its own disadvantage. While having the potential to improve image quality for low-dose data by using an accurate imaging model, pre-log domain methods suffer slow convergence in practice due to the nonlinear transformation from the image to measurements. In contrast, post-log domain methods have fast convergence speed but the resulting image quality is suboptimal for low-dose CT data because the log transformation is extremely unreliable for low-count measurements and undefined for negative values. This paper proposes a hybrid method that integrates the pre-log model and post-log model together to overcome the disadvantages of individual pre-log and post-log methods. We divide a set of CT data into high-count and low-count regions. The post-log weighted least squares model is used for measurements in the high-count region and the pre-log shifted Poisson model for measurements in the low-count region. The hybrid likelihood function can be optimized using an existing iterative algorithm. Computer simulations and phantom experiments show that the proposed hybrid method can achieve faster early convergence than the pre-log shifted Poisson likelihood method and better signal-to-noise performance than the post-log weighted least squares method.

Correspondence to: Jinyi Qi.

G. Wang is now with Department of Radiology, School of Medicine, University of California - Davis, Sacramento, CA 95817 USA
W. Wang is now with Department of Radiation Oncology, Columbia University, USA

Index Terms

low-dose CT; image reconstruction; iterative algorithm; noise model; shifted Poisson; weighted least squares

I. Introduction

X-ray computed tomography (CT) has found extensive clinical applications in cancer, heart, and brain imaging. As CT has been increasingly used for cancer screening [1] and pediatric imaging [2], there is a long-term need to reduce radiation dose of clinical CT scans to as low as reasonably achievable. Statistically efficient tomographic image reconstruction is essential to low-dose CT imaging [3]. Recent studies have shown that iterative image reconstruction algorithms, as compared with traditional analytical algorithms, hold the promise to reduce radiation dose and improve low-dose CT image quality [4], [5].

There are two categories of tomographic image reconstruction methods for CT: (1) pre-log domain methods and (2) postlog domain methods. In the pre-log domain methods, a CT image is directly reconstructed from the raw measurements using either the complex compound Poisson likelihood [6], [7] or an approximate statistical model such as the shifted Poisson model [8]. In the the post-log domain methods, a log transformation is first taken on the ratio between the raw measurements and the blank scan to generate post-log sinogram data that represent line integrals. The filtered backprojection (FBP) reconstruction or penalized weighted least squares (PWLS) method can then be used to reconstruct the CT image from the sinogram data [9], [10].

Because the line-integral model is linear, post-log methods are relatively simpler and more popular for CT image reconstruction [3], [9], [10]. The linear model leads to more efficient computation and faster convergence in iterative image reconstruction. While the methods work well in conventional CT imaging, they are not optimal for low-dose CT data in which the count level in x-ray detector bins is very low (i.e. high noise) and electronic noise may even render some detector bins to have negative values. In these situations, the log transformation for sinogram generation in the post-log methods is very sensitive to noise and the results become extremely unreliable. For negative measurements, the logarithm cannot even be calculated. As a result, artifacts are often introduced in the reconstructed image, which limits the capability of post-log domain methods for CT dose reduction.

To reduce noise-induced artifacts, post-log domain sinograms can be first smoothed by statistical methods prior to tomographic image reconstruction [11], [12]. However, the sinograms after smoothing may still be either noisy if undersmoothed or biased if over-smoothed. Furthermore, the benefit of iterative image reconstruction can be maximized if both noise and spatial correlations in the smoothed sinograms are modeled properly. However, accurate and efficient modeling of noise and correlations in the post-smoothed sinogram is difficult because noise propagation is complicated and the imaging system is spatially variant.

To avoid the difficulty in the log transformation, pre-log domain methods operate on raw CT measurements directly. The methods can utilize an accurate or well-approximated statistical model of measurement noise (e.g. the shifted Poisson model [8]) and have the potential to improve image quality in low-dose CT [13]. However, the data model for x-ray transmission is nonlinear, resulting in a complex optimization problem to solve. Although existing optimization approaches, such as the ordered subsets separable paraboloidal surrogate (OS-SPS) algorithm [10], [14], can be efficiently implemented, these algorithms converge slowly to the penalized likelihood solution because of the nonlinear transformation between the pre-log domain and image domain. As a result, the image estimate obtained in a practically feasible time may not achieve the optimal performance of a fully converged solution.

In this paper, we propose a hybrid method that combines pre-log and post-log domain data together to accelerate CT image reconstruction and to improve image quality. While the pre-log domain methods and post-log domain methods have been proposed individually for CT image reconstruction, the hybrid method proposed here presents an innovative and unique reconstruction method because it overcomes the disadvantage of the individual post-log and pre-log methods. The basic idea is to divide a set of CT data into two subsets, a “high-count” subset and “low-count” subset. The division can be performed either by comparing the raw measurements with a threshold parameter or using a transform of the CT data (such as a denoised sinogram or forward projection of an initial reconstruction). Then for the high-count data bins, we take the logarithm and use the post-log weighted least squares formulation to achieve fast convergence; for the low-count data bins, we do not take the logarithm and use the prelog shifted Poisson model to exploit the benefit of statistical noise modeling. With a proper selection of the threshold parameter, we expect the hybrid method can achieve a fast convergence similar to the post-log weighted least squares method but with improved image quality similar to that of the pre-log shifted-Poisson method. A hybrid Poisson/polynomial objective function was also used for PET/SPECT transmission scans to reduce exponential operations [15].

This paper is organized as follows. We start with a brief description of CT data model, existing pre-log domain and post-log domain methods in Section II and then describe the proposed hybrid method in Section III. Section IV and V respectively present computer simulation and phantom experiment studies comparing the hybrid method with pre-log domain and post-log domain methods. Finally conclusions are drawn in Section V.

II. Tomographic Image Reconstruction for CT

A. CT Data Model

The statistical process of CT imaging is complex and noise generally follows compound Poisson distributions [6]. In practice, it is accepted that after system calibration and data correction, CT data can be modeled by the sum of independent Poisson random variables generated by x-ray flux and white Gaussian noise accounting for electronic noise in the measurement [7], [11]. The statistical model of the random variable Y_i measured by detector bin i of a CT scanner can be described as

$$Y_i \sim Poisson\ (\bar{y}_i(\boldsymbol{x})) + Gaussian\ \left(0, \sigma_e^2\right) \quad (1)$$

where σ_e denotes the standard deviation of electronic noise and $\bar{y}_i(\boldsymbol{x})$ is the expected projection data related to the image of linear attenuation coefficient, $\boldsymbol{x}$, through a nonlinear transformation [10],

$$\bar{y}_i(\boldsymbol{x}) = b_i\ exp\ (-[\boldsymbol{A}\boldsymbol{x}]_i) + s_i \quad (2)$$

with b_i being the blank scan measurement in detector bin i and s_i the mean of background measurement (e.g. scattered photons). $[\boldsymbol{A}\boldsymbol{x}]_i$ denotes the line integral through $\boldsymbol{x}$ along the ith measurement with the (i, j)th element of the system matrix $\boldsymbol{A}$ being the line length of x-ray photons passing through voxel j along the ith measurement [16], [17].

Modeling the effect of electronic noise is important for low-dose CT image reconstruction. While there is no simple analytical form for the likelihood function of the combined Poisson and Gaussian model in (1), the sum, after adding a constant, can be approximated by a Poisson distribution [8], [11], i.e.,

$$\hat{Y}_i = \left[Y_i + \sigma_e^2\right]_+ \sim Poisson\ \left(\bar{y}_i(\boldsymbol{x}) + \sigma_e^2\right), \quad (3)$$

where $[\cdot]_+$ thresholds any negative value to zero. This is commonly referred to as the shifted Poisson model. The first two moments (mean and variance) of the shifted Poisson model match exactly those of the Poisson-Gaussian model in (1). The shifted Poisson model is more attractive in practice than other more complex models because its computation is more tractable.

B. Pre-log Domain Method

Let us denote the realizations of random variable Y in all detector bins by $\boldsymbol{y} \in IR^{n_i \times 1}$ with n_i being the number of detector bins. A pre-log domain method reconstructs the image $\boldsymbol{x}$ either from the measurement $\boldsymbol{y}$ using a complex likelihood function [6] or from the shifted data

$$\hat{\boldsymbol{y}} = [\boldsymbol{y} + \sigma_e^2]_+ \quad (4)$$

using the more tractable shifted Poisson model [8], [11]. For the latter, the image estimate is obtained by maximizing the log likelihood function of the shifted Poisson model,

$$\hat{\boldsymbol{x}} = arg\ \max_{\boldsymbol{x} \geq \boldsymbol{0}} \sum_{i=1}^{n_i} \left[\hat{y}_i\ log\ (\bar{y}_i(\boldsymbol{x}) + \sigma_e^2) - \left(\bar{y}_i(\boldsymbol{x}) + \sigma_e^2\right)\right] - \beta U(\boldsymbol{x}) \quad (5)$$

where $U(\boldsymbol{x})$ is an image roughness penalty and β controls the strength of the regularization. $U(\boldsymbol{x})$ is generally defined on the intensity difference between neighboring pixels [18],

$$U(\boldsymbol{x})=\sum_j \sum_{k\in N_j} w_{jk}\psi_\delta(x_j - x_k) \quad (6)$$

where $\psi_\delta(t)$ is a penalty function and δ is a parameter that controls the smoothness of the penalty function, w_{jk} is the weighting factor related to the distance between pixel j and pixel k in the neighborhood N_j. An example of $\psi_\delta(t)$ is the Huber function [19],

$$\psi_\delta(t)=\begin{cases} \frac{1}{2}t^2, & |t|\le\delta \\ \delta|t|-\frac{\delta^2}{2}, & otherwise. \end{cases} \quad (7)$$

The optimization problem in (5) can be solved by the separable paraboloidal surrogate (SPS) algorithm [20] with acceleration by ordered subsets (OS) [14], [21]. The advantage of the pre-log domain methods is that an accurate noise model is available, which can benefit low-count CT image reconstruction. However, due to the nonlinearity of the expected data $\bar{\boldsymbol{y}}(\boldsymbol{x})$ with respect to the image $\boldsymbol{x}$, the associated computation can be more costly and the convergence of a pre-log method is generally slower than that of the post-log domain method described below.

C. Post-log Domain Method

Post-log domain methods employ a log transformation to remove the nonlinearity in (2) and simplify the reconstruction to a linear problem. Specifically, a noisy measurement of the line integral $\bar{\ell}_i(\boldsymbol{x}) = [\boldsymbol{A}\boldsymbol{x}]_i$ can be obtained by

$$\hat{\ell}_i=log\,\frac{b_i}{max(y_i - s_i, \varepsilon)}, \quad (8)$$

where ε is a small value (e.g. 0.1) to avoid dividing by zero and also remove negative values. The image $\boldsymbol{x}$ can then be reconstructed from $\hat{\boldsymbol{\ell}}$ by the following penalized weighted least squares (PWLS) formulation [9], [10],

$$\hat{\boldsymbol{x}}=arg\,\min_{\boldsymbol{x}\ge\boldsymbol{0}} \sum_{i=1}^{n_i} \frac{w_i}{2}\left(\hat{\ell}_i - \bar{\ell}_i(\boldsymbol{x})\right)^2 + \beta U(\boldsymbol{x}) \quad (9)$$

where the weighting factor $\{w_i\}$ approximates the variance inverse of $\hat{\ell}$ that is derived from the Poisson model,

$$w_i=\frac{(y_i - s_i)^2}{y_i+\sigma_e^2}. \quad (10)$$

The post-log reconstruction problem defined in Eq. (9) can be solved either by the OS-SPS algorithm [10] or by other algorithms [9], [22]. Its convergence is usually fast. However, the log transformation can become unstable when the signalto-noise ratio (SNR) of $y_i - s_i$ is low. Noise in $\boldsymbol{y}$ can be amplified in $\hat{\boldsymbol{\ell}}$ by the log transformation and the resulting postlog sinogram can be biased; both introduce artifacts in the reconstructed images. These issues substantially limited the performance of post-log domain reconstruction methods for low-dose CT.

III. Proposed Hybrid Method

Both the pre-log domain method and post-log domain method have their own advantages and disadvantages. Here we propose a hybrid method to overcome the disadvantages of the individual pre-log and post-log methods.

A. Mathematical Formulation

The basic idea of the proposed method is to use a hybrid log-likelihood function to combine the benefits of pre-log and post-log methods. The hybrid log-likelihood function has the following form

$$L(\boldsymbol{x}) = \sum_{i=1}^{n_i} h_{i,\tau}\left([\boldsymbol{A}\boldsymbol{x}]_i\right), \tag{11}$$

where $h_{i,\tau}(\ell)$ denotes the data fidelity for detector bin i with τ as a threshold parameter for choosing either the shift Poisson model or the weighed least squares model for the data. For a specific detector bin i, if the measurement y_i is less than the threshold τ, the shifted Poisson model will be chosen to take advantage of statistical noise modeling in the prelog domain and avoid noise amplification caused by the log transformation; if the measurement y_i is greater than τ, the log transformation for the post-log sinogram generation is expected to be robust and the weighted least squares model will be used to take advantage of fast convergence of the PWLS method.

Mathematically $h_{i,\tau}(\ell)$ is given by

$$h_{i,\tau}(\ell) = \begin{cases} \tilde{y}_i(\ell) - \left([y_i + \sigma_e^2]_+\right) log\, \tilde{y}_i(\ell), & y_i < \tau, \\ \frac{1}{2} w_i \left(\hat{\ell}_i - \ell\right)^2, & y_i \geq \tau, \end{cases} \tag{12}$$

where

$$\tilde{y}_i(\ell) \triangleq b_i exp\,(-\ell) + s_i + \sigma_e^2. \tag{13}$$

The post-log sinogram $\hat{\ell}_i$ is given in (8) and the weight w_i in (10).

The hybrid method seeks the following penalized likelihood estimate

$$\hat{\boldsymbol{x}}=arg\min_{\boldsymbol{x}\geq\mathbf{0}}\sum_{i=1}^{n_i}h_{i,\tau}\left([\boldsymbol{A}x]_i\right)+\beta U(\boldsymbol{x}). \quad (14)$$

We use the same regularization $U(\boldsymbol{x})$ defined in (6) for the hybrid method. It is easy to verify that the hybrid loglikelihood function reverts back to the post-log PWLS model when $\boldsymbol{\tau} = 0$, and to the pre-log shifted Poisson model when $\boldsymbol{\tau} = \infty$. By properly choosing the threshold value $\boldsymbol{\tau}$, the hybrid method can converge much faster than the existing method that uses pre-log domain data ($\boldsymbol{\tau} = \infty$) and result in better image quality at convergence compared to the post-log domain method ($\boldsymbol{\tau} = 0$).

B. Implementation

A graphical description of the hybrid method is given in Figure 1. The implementation consists of two steps.

At Step 1, the threshold parameter $\boldsymbol{\tau}$ is determined using the standard deviation of electronic noise and count level of the CT data. Two masks are then obtained to partition the CT data into a low-count region (Mask 1) and a high-count region (Mask 2). Then pre-log data and post-log data are extracted based on the two masks. While we use a simple threshold method, the pre- and post-log masks can also be generated by other means, e.g., based on a forward projection of a segmented image.

At Step 2, for any detector bin that is assigned to use pre-log data, the shifted Poisson model is employed for data fidelity; for any detector bin assigned to use post-log data, the weighted least squares formulation is employed. The partial pre-log data and post-log data are combined together for the final penalized likelihood image reconstruction.

Existing iterative optimization algorithms, such as OS-SPS algorithm [14] and its accelerated versions by the momentum approach [23], can be used to solve the optimization problem.

IV. Validation Using Computer Simulation

A. Simulation Setup

We conducted a computer simulation study to validate the proposed hybrid method for CT image reconstruction. A CT scanner [12] was simulated for 2D CT imaging. A total of 984 fan-beam projections for a 360° rotation and 888 bins for each projection view were used. The distance from the detector face to the center of rotation was 408 mm and the distance from the source to the detector face was 949 mm. The detector cell spacing was 1.0239 mm. The field of view was set to 500 mm.

The simulation used a digital shoulder phantom of image size 128 × 128. The phantom contains bone and water back-ground as shown in Fig. 2. Linear attenuation coefficients of bone and water were simulated at 80 keV. For each detector bin, the number of incident photons was set to $b_i = 10^4$ and 3% uniform scattered background was also simulated. No

bow-tie filtration was simulated. Poisson noise was introduced to the pre-log data. Electronic noise was simulated by Gaussian noise with zero mean and variance $\sigma_e^2=40$.

B. Reconstruction Methods to Compare and Evaluation Metrics

The noisy CT data from the simulation were reconstructed using three different methods: the penalized weighted least squares (PWLS) method in the post-log domain, the shifted Poisson (SP) method in the pre-log domain, and the proposed hybrid method integrating both pre-log data and post-log data. The Huber penalty with $\delta = 0.001$ was used for regularization. The δ value was chosen to achieve a balance between approximating the total variation (TV) penalty and avoiding the nonsmooth differentiation of the TV. The OS-SPS algorithm [14] with 41 subsets and 250 iterations was used to optimize the objective function for all three methods. The initial estimate was an uniform image with a linear attenuation coefficient of 0.18 cm^{-1} in all reconstructions.

Convergence rate and image quality of different methods were assessed using the image SNR as a function of the iteration number. Image SNR is defined by

$$SNR(\boldsymbol{x}^n) = -10\,log_{10}\frac{\|\boldsymbol{x}^n - \boldsymbol{x}_{true}\|^2}{\|\boldsymbol{x}_{true}\|^2} \quad (15)$$

where $\boldsymbol{x}^n$ is the image estimate at iteration n obtained with one of the three reconstruction methods and $\boldsymbol{x}_{\text{true}}$ denotes the true CT image.

C. Results

Fig. 3 show the reconstructed images by the three different methods: PWLS, SP and hybrid method ($\tau = 64$) with the regularization parameter $\beta = 2^{12}$ which was selected by maximizing the image SNR for all three methods. Fig. 3(a)-(c) shows the reconstructions with 50 iterations and Fig. 3(d)-(f) show the images with 250 iterations. At iteration 50, the reconstructed image by the hybrid method (Fig. 3(c)) achieves a substantially higher SNR than those by the PWLS and SP (Fig. 3(a) and (b)), and the same is true for reconstructed images with 250 iterations. The hybrid method at iteration 50 even achieved an higher image SNR than the other two methods at iteration 250. To put this into perspective, we consider reconstruction of a 3D CT image on a 512×512×144 voxel grid from 2400 projections of 896 channels × 80 rows. One forward and back projections take about 15 seconds on a NIVIDIA GeForce GTX 1080 Ti GPU. The SP method with 250 iterations would need more than one hour to complete the reconstruction, whereas the proposed method with 50 iterations would only take about 13 minutes and result in improved image quality.

Figure 4 shows the comparison of image SNR of the three different methods by varying the number of incident photons b_i. All reconstructions were obtained with 50 iterations. The τ value in the hybrid method was $\tau = 64$ for $b_i = 10^4$ and linearly scaled by the number of photons for other count levels. Compared with PWLS, the SP method did not improve image SNR at the low iteration number n =50 due to its slow convergence. In contrast, the hybrid method brought a significant SNR improvement over PWLS without running more

iterations. The PWLS method achieved a SNR of 19.78 dB at $b_i = 12\times10^3$ and the hybrid method achieved a similar SNR (19.79 dB) at $b_i = 6\times10^3$. With PWLS as the baseline method, the hybrid method is projected to achieve a 2-fold dose reduction without compromising image quality.

Figure 5 plots the image SNR as a function of the iteration number for the three methods for reconstructing the data of the count level $b_i = 10^4$. The PWLS reconstruction converges faster at early iterations than the SP does, but its SNR at convergence is lower than that of the SP. In comparison, the hybrid method ($\tau = 64$) combines the advantages of both PWLS and SP: the hybrid reconstruction is as fast as the PWLS at early iterations and is also able to achieve a higher SNR than both the PWLS and SP methods.

D. Effect of the Threshold Parameter on the Hybrid Method

The effect of the threshold parameter τ on the convergence speed of the hybrid method is also shown in Figure 5. The PWLS method is equivalent to the hybrid method with $\tau = 0$. As τ was increased to $\tau = 50$, the hybrid method achieved a higher SNR than the PWLS, although the convergence speed became a little bit slower. The SNR of the hybrid method was further improved when τ was increased to 64. When τ continued to increase to 100, the convergence speed became much slower and the image SNR dropped when compared to that of $\tau = 64$. The hybrid method would become close to the SP method if τ takes a very large value.

To further understand the behavior of the hybrid method, Fig. 6 shows the image SNR of the reconstructions with different iterations as a function of the threshold parameter τ. Figure 6(a) shows the results for reconstructions with 50 iterations. The SNRs of PWLS and SP reconstructions are included as straight lines for comparisons. When τ is close to zero, very few detector bins are selected for using the prelog model and the hybrid method is essentially the same as the PWLS reconstruction. When τ is in the middle range, the hybrid model brings the benefit of the pre-log domain noise modeling for low-count detector bins to achieve higher image SNR in image reconstruction. As τ further increases, the hybrid method becomes closer to the pre-log SP method - starts to suffer from slow convergence and results in lower image SNR.

Figure 6(b) and 6(c) show the comparison at two larger number of iterations ($n = 250$ and $n = 2500$, respectively) that get closer to the convergent solution of each reconstruction. The results show that with more iterations, the SNR reduction due to the increase of τ became less. In all cases, the hybrid method still performed the best with a proper τ. It is anticipated that at the convergent solution (which requires thousands of iterations to achieve), the SP method will set the upper bound of the hybrid method.

V. Validation Using a Physical Phantom Experiment

A. Physical Phantom Experiment

A physical shoulder phantom was scanned in a Toshiba Aquilion ONE CT scanner at two dose levels: a high-dose scan at 300 mAs and low-dose scan at 5 mAs. The scanner has a total of 1,200 fan-beam projections for a 360° rotation, 896 radial bins for each projection

view, and 80 segments along the axial direction. A standard bow-tie filter was used during the scan. One axial slice was taken for the study in this work. The transaxial field of view was 500 mm and the image array for reconstruction was 512 × 512.

The high-dose data (300 mAs) were reconstructed using the weighted least square reconstruction method with 100 iterations and the result is shown in Figure 7. The image was used as $\boldsymbol{x}_{\text{true}}$ in (15) to calculate the image SNR of reconstructions of the low-dose (5 mAs) data.

In addition, the shoulder phantom was scanned repeatedly ($N = 1200$) with the x-ray source and detector fixed at their horizontal positions to verify the shifted-Poisson model. The mean and variance of the pre-log data calculated from the repeated measurements were fitted to a linear function according to the shifted-Poisson distribution. The resulting slope of the linear fit is 1.006 with $R^2 = 0.9910$, which indicates the variance of the pre-log data can be well predicted by the shifted-Poisson model.

B. Comparison of Reconstruction Methods

The three different reconstruction methods (PWLS, SP and hybrid) were compared for reconstructing the low-dose data. In all reconstructions, beam hardening correction was applied. The OS-SPS algorithm with 40 subsets was used in all reconstructions with a uniform initial image.

Figure 8 (a-c) shows the images reconstructed by the three methods with 15 iterations and Figure 8 (d-f) shows the reconstructions with 50 iterations. The regularization parameter β was chosen to be 2^{10} in all three methods to maximize the SNR approximately. The threshold parameter in the hybrid method was set to $\tau = 40$. Similar to the simulation results, the hybrid method achieved a higher image SNR than the other two methods (PWLS and SP).

Figure 9 shows the image SNR as a function of the iteration number for each method. At early iterations, the image SNR of the pre-log SP method increases slowly, while both the PWLS and hybrid methods improve the SNR at a much faster rate thanks to the linear imaging model of post-log data. At later iterations, the SNR of the PWLS method stops increasing, while the SP method continued to improve the SNR thanks to the accurate noise modeling of the pre-log data. The hybrid method combined the advantages of PWLS and SP and achieved a high SNR very fast.

These results indicate that the hybrid method was able to combine the advantages of post-log and pre-log domain data to achieve higher image quality than the PWLS method and more efficient reconstruction than the SP method.

C. Effect of the Model Parameters

We investigated the effect of the threshold parameter τ and regularization parameter β on the image SNR for the hybrid method in the physical phantom study.

Figure 10 shows the image SNR of the hybrid reconstruction with 15 iterations as a two-dimensional function of the regularization parameter β and threshold parameter τ. We varied the value of τ from −40 to 6000. These two extreme τ values corresponded to the PWLS and SP reconstructions, respectively. The optimal values of τ fell into the range between $\tau = 20$ and $\tau = 50$ for different β values varying from a very small value $\beta = 2^{-10}$, which resulted in a nearly unregularized image estimate, to a large value $\beta = 2^{14}$, which resulted in an over-smoothed image estimate. The results here demonstrate that the optimal value of τ was nearly independent of β for achieving the best image SNR.

Figure 11(a) shows the 1-D plot of the image SNR as a function of the threshold parameter τ in the hybrid method with 15 iterations and a fixed $\beta = 2^{10}$. For a fixed iteration number of 15, the SP method could not fully exploit the benefit of pre-log domain noise modeling and performed even worse than the PWLS reconstruction. The hybrid method overcame the limitation of SP by combining post-log and pre-log data and achieved the highest image SNR at $\tau = 40$. As τ further increases, the convergence speed of the algorithm becomes slower, resulting in a reduction of SNR at the fixed number of iterations. Figure 11(b) shows the same plot for a larger number of iterations ($n = 50$). The SNR of SP reconstruction became higher but was still lower than that of the hybrid reconstruction with a proper τ value.

Figure 12 compares the image SNR of the PWLS, SP and hybrid reconstructions at 15 iterations by varying the regularization parameter β in each method. The threshold parameter τ in the hybrid method was 40. The maximal image SNR was achieved at $\beta = 2^{11}$ for all three methods. The hybrid method obtained the highest image SNR among different methods. For comparison, the SNR curve of SP with 50 iterations is also shown. With only 1/3 number of iterations, the hybrid reconstruction achieved a even higher SNR than the SP reconstruction. It is worth noting that the SP method would have achieved higher SNR if converged solutions were obtained; however, it would require much more iterations and computational time that may not be practical for clinical applications.

VI. Conclusion

We have presented a new hybrid method that combines pre-log and post-log data together for low-dose CT image reconstruction. The proposed method can retain the high image quality offered by the pre-log data model, while overcoming the slow convergence of the pre-log domain SP method. Results from a computer simulation as well as a physical phantom experiment demonstrated that the hybrid method achieved faster convergence than the pre-log SP method and better image quality than the PWLS method. Computer simulation also shows that the hybrid method can achieve a 2-fold dose reduction as compared with the PWLS method. Future work will include more task-specific image quality assessment and development of an automated method to select the threshold parameter.

Acknowledgments

This work was supported in part by the National Institute of Biomedical Imaging and Bioengineering under grant no. R01EB000194.

References

1. Bach PB, Mirkin JN, Oliver TK, Azzoli CG, Berry DA, Brawley OW, Byers T, Colditz GA, Gould MK, Jett JR, Sabichi AL, Smith-Bindman R, Wood DE, Qaseem A, Detterbeck FC. Benefits and harms of CT screening for lung cancer: a systematic review. Journal of American Medical Association. 2012; 307(22):2418–2429.
2. Singh S, Kalra MK, Shenoy-Bhangle AS, Saini A, Gervais DA, Westra SJ, Thrall JH. Radiation Dose Reduction with Hybrid Iterative Reconstruction for Pediatric CT. Radiology. 2012; 263(2): 537–546. [PubMed: 22517962]
3. Beister M, Kolditz D, Kalender WA. Iterative reconstruction methods in X-ray CT. Physica Medica. 2012; 28(2):94–108. [PubMed: 22316498]
4. Singh S, Kalra MK, Hsieh J, Licato PE, Do S, Pien HH, Blake MA. Abdominal CT: Comparison of Adaptive Statistical Iterative and Filtered Back Projection Reconstruction Techniques. Radiology. 2010; 257(2):373–83. [PubMed: 20829535]
5. Prakash P, Kalra MK, Kambadakone AK, Pien H, Hsieh J, Blake MA, Sahani DV. Reducing abdominal CT radiation dose with adaptive statistical iterative reconstruction technique. Investigative Radiology. 2010; 45(4):202–10. [PubMed: 20177389]
6. Whiting BR, Massoumzadeh P, Earl OA, O'Sullivan JA, Snyde DL, Williamson JF. Properties of preprocessed sinogram data in x-ray computed tomography. Medical Physics. 2006; 33(9):3290–3303. [PubMed: 17022224]
7. Snyder DL, Hammoud AM, White RL. Image recovery from data acquired with a charge-coupled-device camera. Journal of the Optical Society of America A. 1993; 10(5):1014–1023.
8. Yavuz M, Fessler JA. Statistical image reconstruction methods for randoms-precorrected PET scans. Medical Image Analysis. 1998; 2(4):369–378. [PubMed: 10072203]
9. Thibault JB, Sauer KD, Bouman CA, Hsieh J. A three-dimensional statistical approach to improved image quality for multislice helical CT. Medical Physics. 2007; 34(11):4526–4544. [PubMed: 18072519]
10. Elbakri IA, Fessler JA. Statistical Image Reconstruction for Polyenergetic X-Ray Computed Tomography. IEEE Transactions on Medical Imaging. 2002; 21(2):89–99. [PubMed: 11929108]
11. La Riviere PJ. Penalized-likelihood sinogram smoothing for low-dose CT. Medical Physics. 2005; 32(6):1676–1683. [PubMed: 16013726]
12. Wang J, Li T, Lu H, Liang Z. Penalized weighted least-squares approach to sinogram noise reduction and image reconstruction for low-dose X-ray computed tomography. IEEE Transactions on Medical Imaging. 2006; 25(10):1272–1283. [PubMed: 17024831]
13. Fu L, Lee TC, Kim SM, Alessio AM, Kinahan PE, Chang Z, Sauer K, Kalra MK, De Man B. Comparison Between Pre-Log and Post-Log Statistical Models in Ultra-Low-Dose CT Reconstruction. IEEE Transactions on Medical Imaging. Mar; 2017 36(3):707–720. [PubMed: 28113926]
14. Erdogan H, Fessler JA. Ordered subsets algorithms for transmission tomography. Physics in Medicine and Biology. 1999; 44(11):2835–51. [PubMed: 10588288]
15. Fessler JA. Hybrid Poisson/polynomial objective functions for tomographic image reconstruction from transmission scans. IEEE Transactions on Image Processing. Oct; 1995 4(1):1439–1450. [PubMed: 18291975]
16. De Man B, Basu S. Distance-driven projection and backprojection in three dimensions. Physics in Medicine and Biology. 2004; 49(11):2463–75. [PubMed: 15248590]
17. Long Y, Fessler JA, Balter JM. 3D forward and back-projection for X-ray CT using separable footprints. IEEE Transactions on Medical Imaging. Nov; 2010 29(11):1839–1850. [PubMed: 20529732]
18. Geman, S., McClure, D. Proceedings of the Statistical Computing Section of the American Statistical Association. Washington, DC, USA: 1985. Bayesian image analysis: an application to single photon emission tomography; p. 12-18.
19. Huber, PJ. Robust Statistics. John Wiley & Sons; New York, NY, USA: 1981.
20. Erdogan H, Fessler JA. Monotonic algorithms for transmission tomography. IEEE Transactions on Medical Imaging. Apr; 1999 18(9):801–814. [PubMed: 10571385]

21. Hudson HM, Larkin RS. Accelerated image reconstruction using ordered subsets of projection data. IEEE Transactions on Medical Imaging. 1994; 13(4):601–609. [PubMed: 18218538]
22. Yu Z, Thibault JB, Bouman CA, Sauer KD, Hsieh J. Fast modelbased X-ray CT reconstruction using spatially nonhomogeneous ICD optimization. IEEE Transactions on Medical Imaging. 2011; 20(1):161–75.
23. Kim D, Ramani S, Fessler JA. Combining ordered subsets and momentum for accelerated X-ray CT image reconstruction. IEEE Transactions on Medical Imaging. 2014; 34(1):167–78. [PubMed: 25163058]

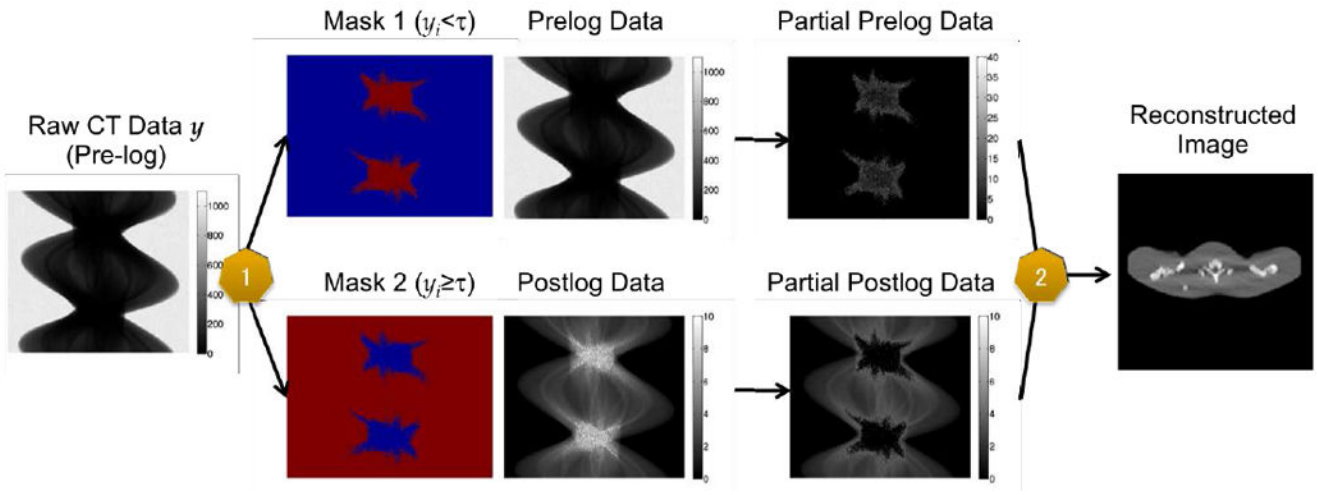

Fig. 1.

Graphical description of the hybrid method with two steps. In step 1, a threshold parameter τ is applied to the raw CT measurements to generate two masks for low-count and high-count data, respectively. Low-count data are kept in the pre-log domain to avoid noise amplification and log transformation is taken on the high-count data. In step 2, the partial pre-log data and post-log data are combined together for a full set of projection data to reconstruct image.

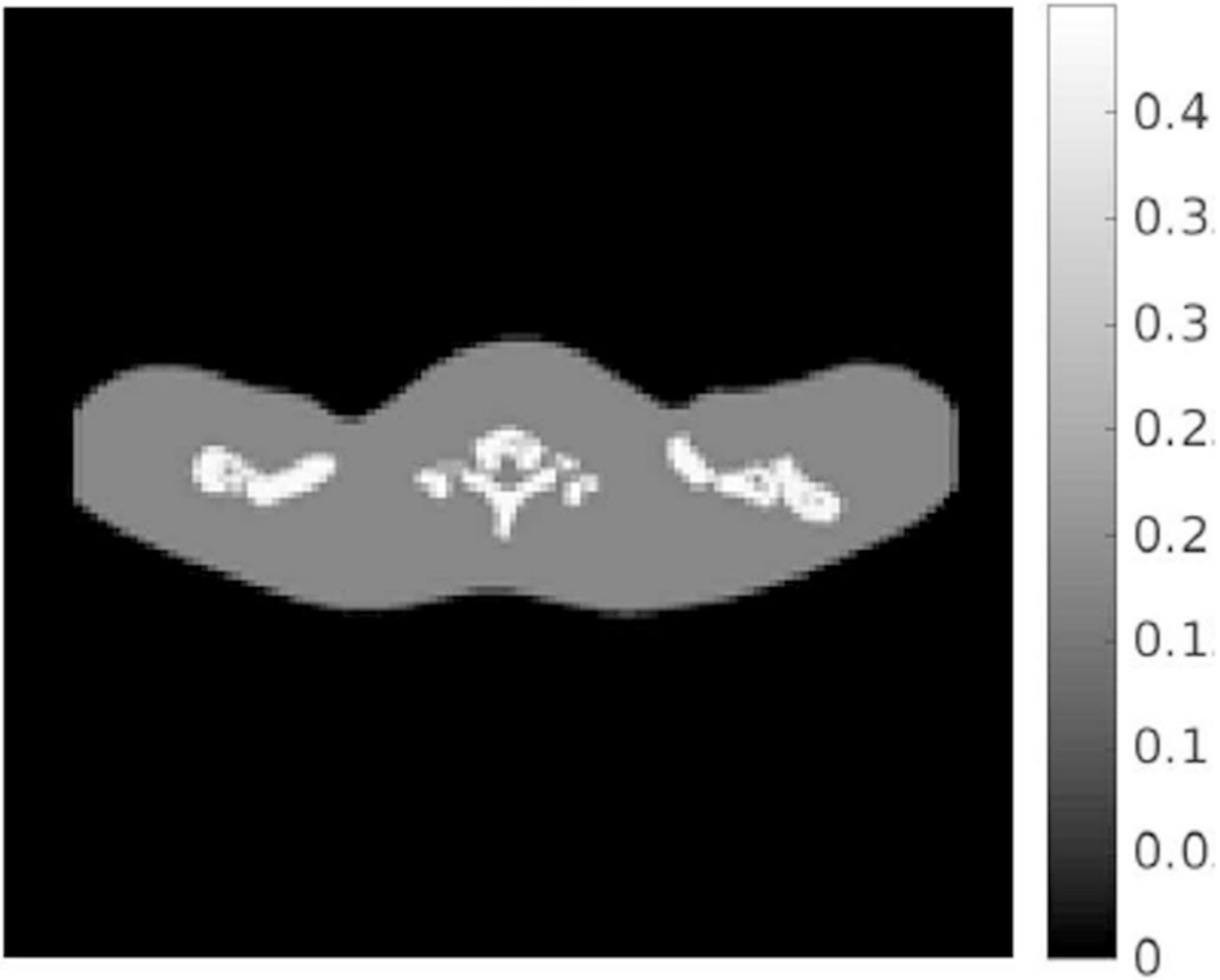

Fig. 2.
The shoulder phantom image used in the computer simulation.

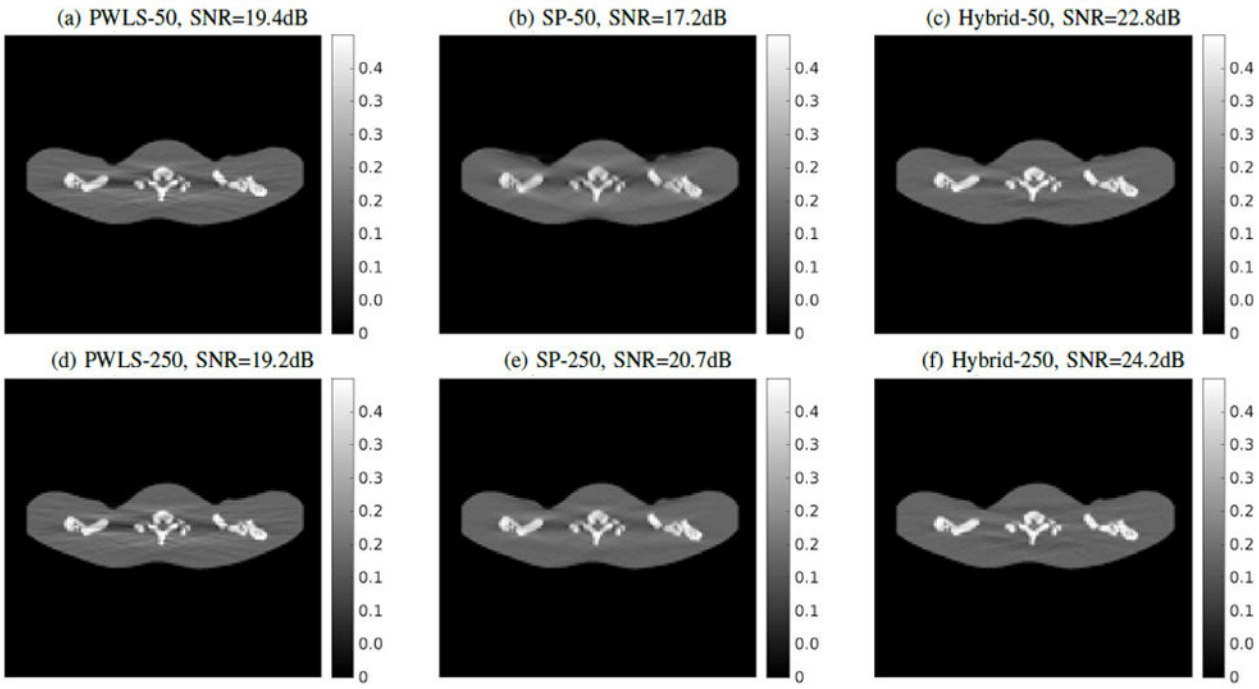

Fig. 3.

Reconstructed images of the simulated shoulder phantom by three different methods (PWLS, SP and Hybrid) using 41 subsets with (a-c) 50 iterations and (d-f) 250 iterations.

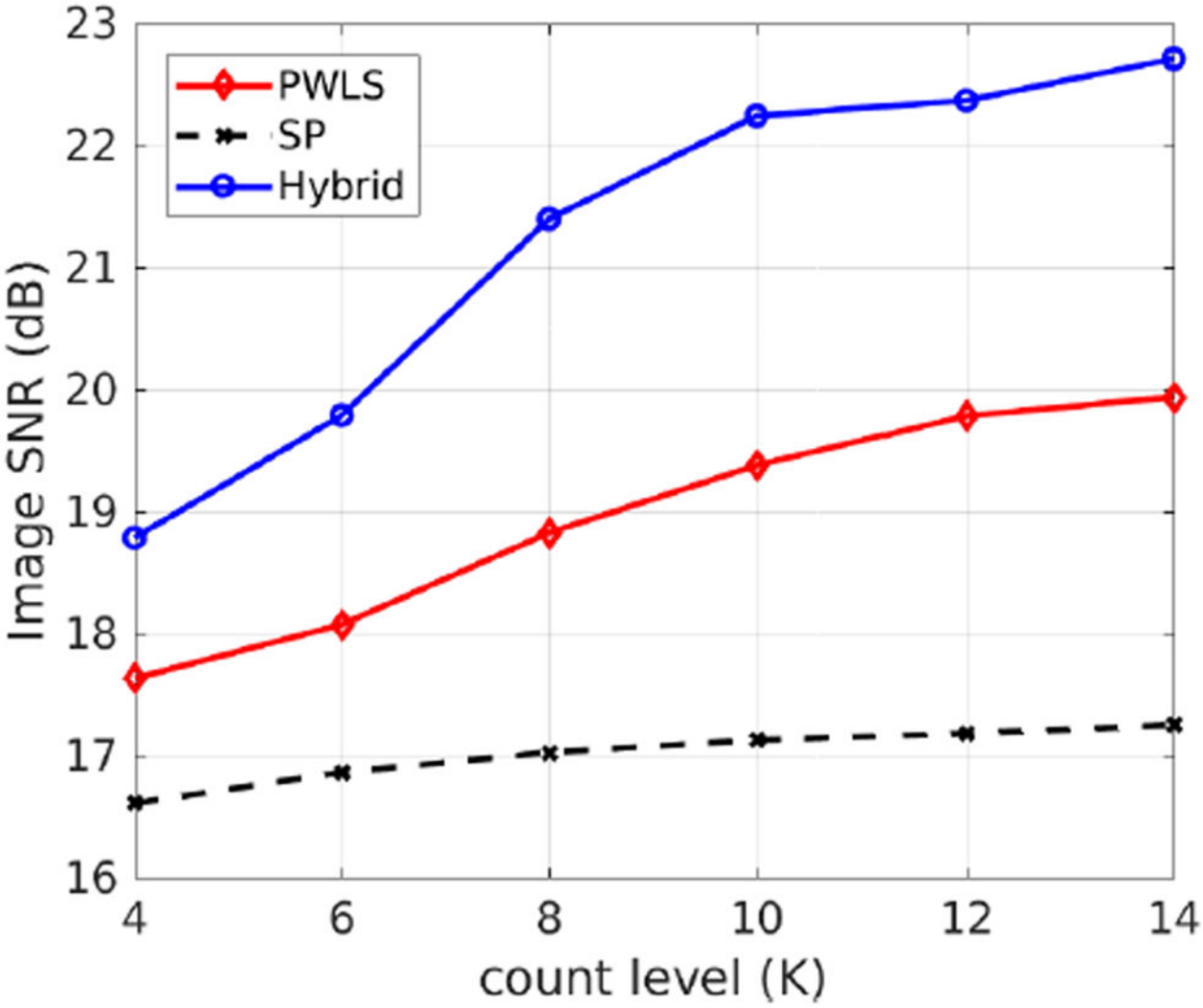

Fig. 4.

Comparison of image SNR of the three reconstruction methods by varying the number of incident photons in the simulation.

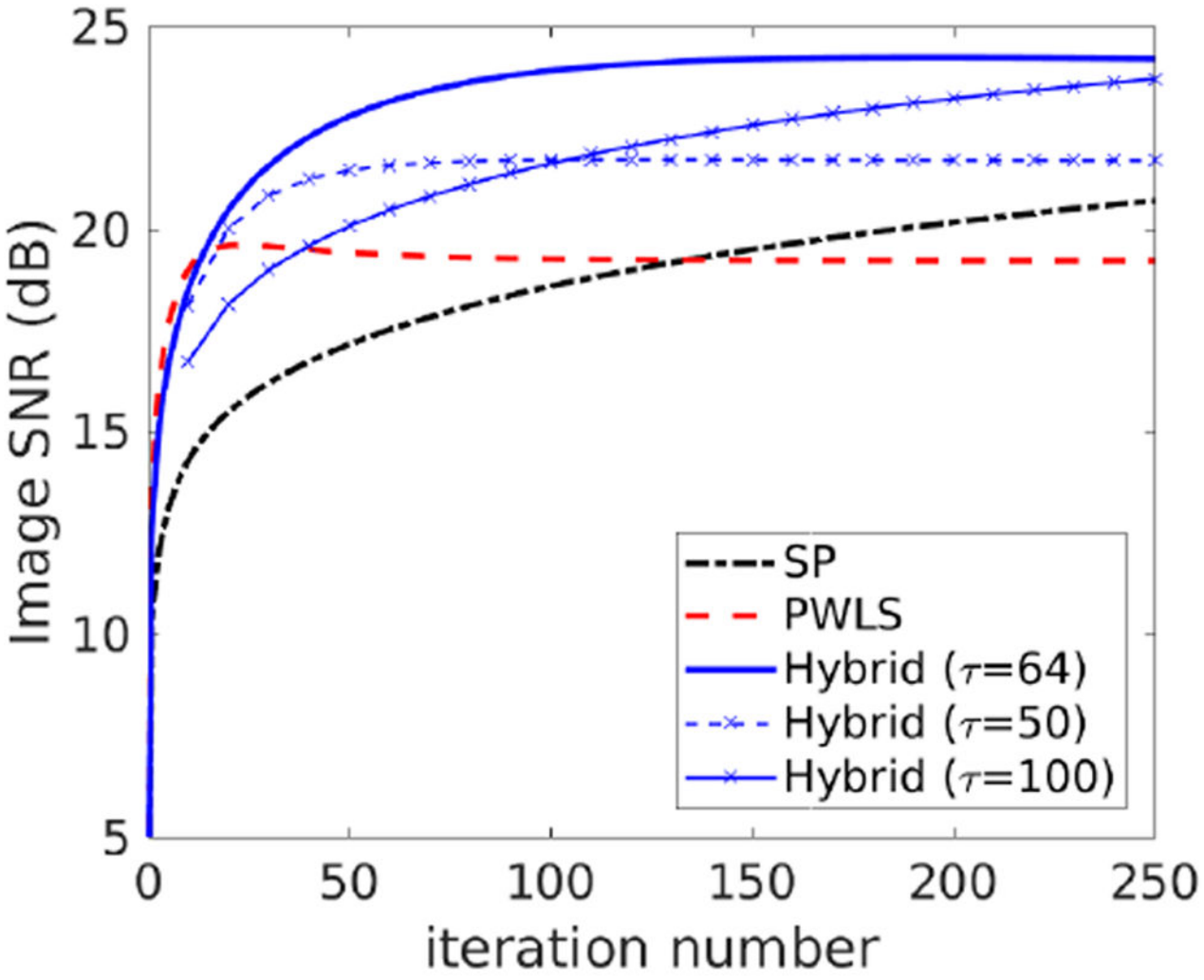

Fig. 5.

Image SNR as a function of the iteration number for reconstructions of the simulated phantom data ($b_i = 10^4$) by different methods. The regularization parameter is $\beta = 2^{12}$.

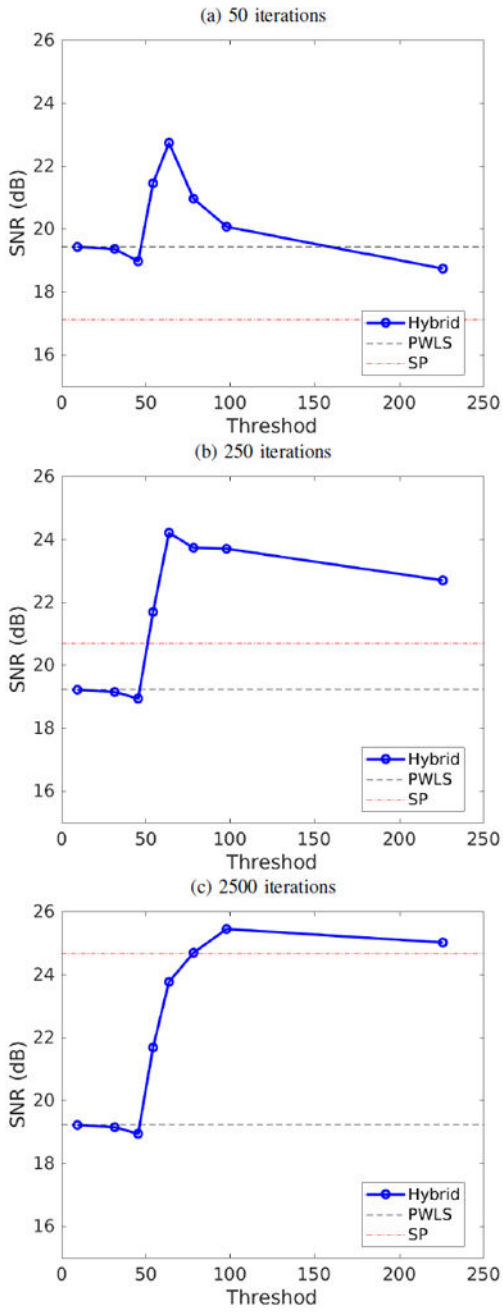

Fig. 6.

Image SNR of the hybrid reconstruction as a function of the threshold τ for the simulated phantom data. (a) all reconstructions with 50 iterations; (b) with 250 iterations; (c) with 2500 iterations.

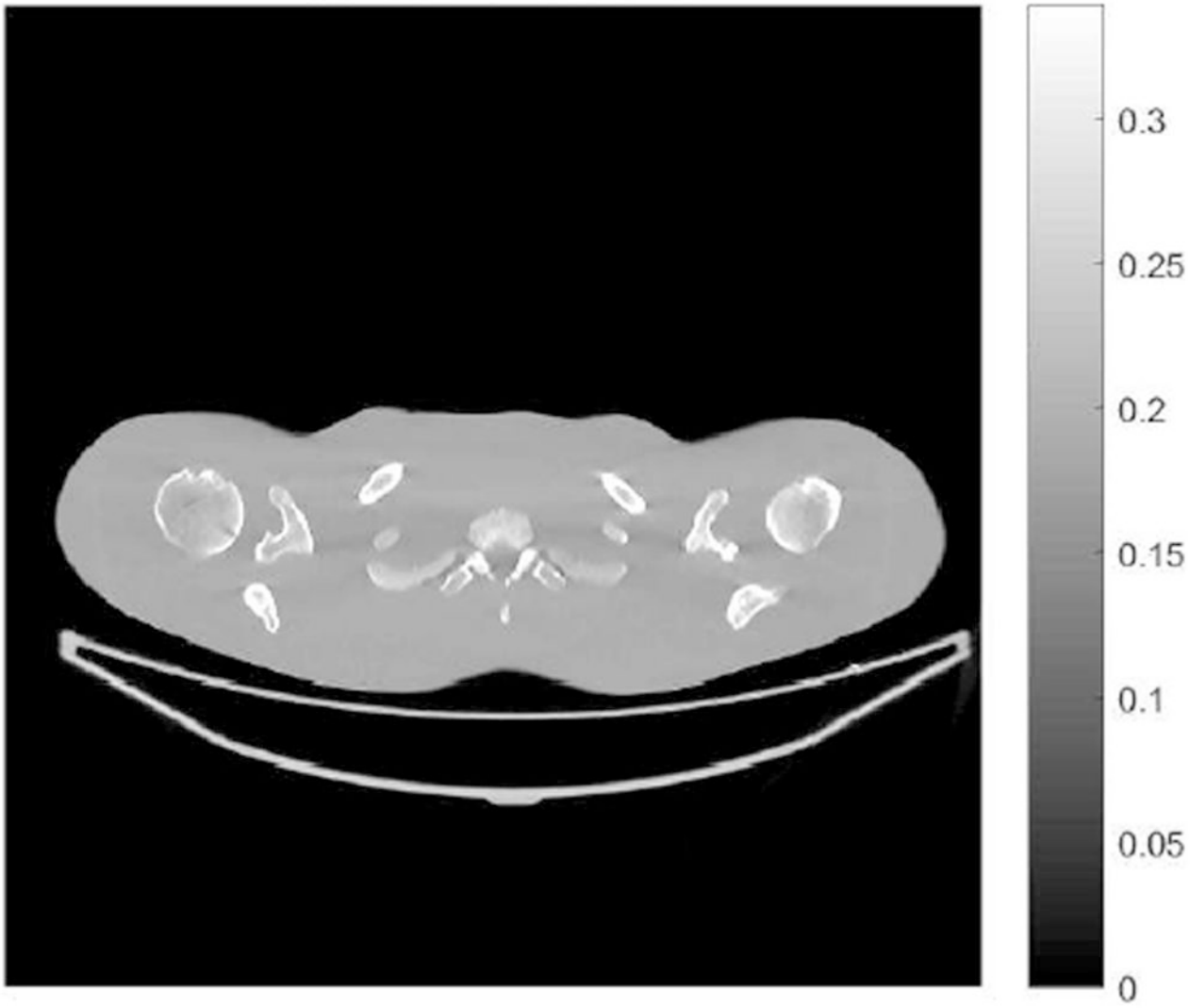

Fig. 7.
High-dose (300 mAs) CT image of the physical shoulder phantom in the experimental study.

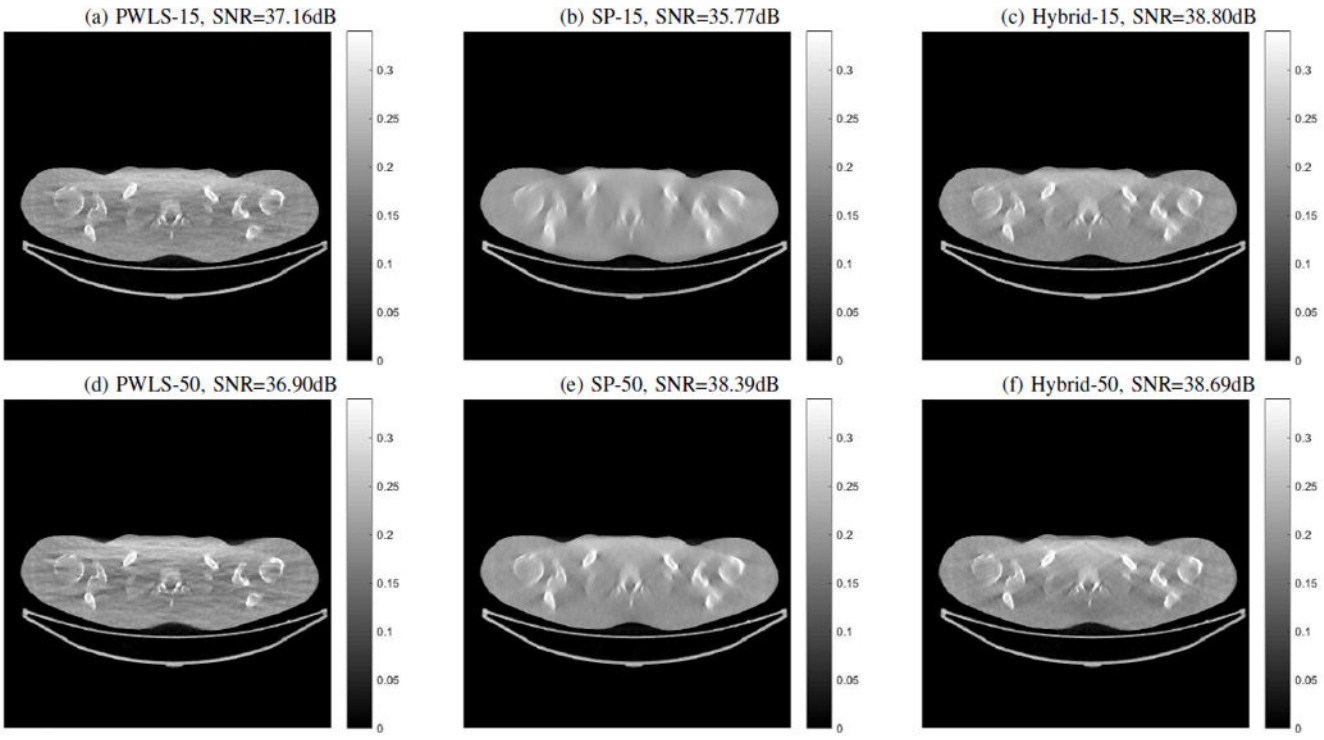

Fig. 8.

Low-dose (5 mAs) reconstructions of the physical shoulder phantom by three different methods (PWLS, SP and Hybrid) using 40 subsets with (a-c) 15 iterations and (d-f) 50 iterations.

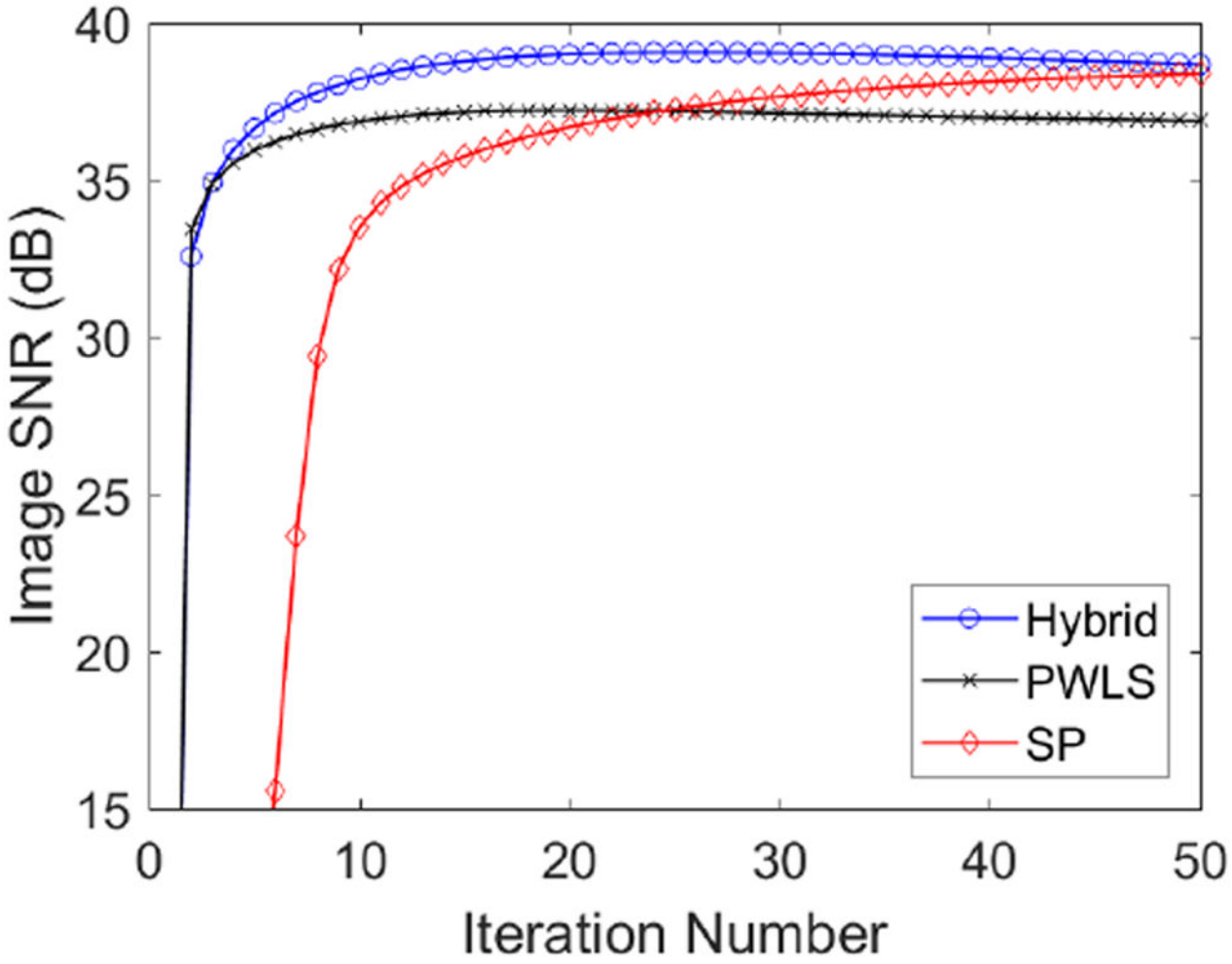

Fig. 9.

Image SNR as a function of iteration number for reconstructions of the physical phantom data by different methods. The regularization parameter is $\beta = 2^{10}$.

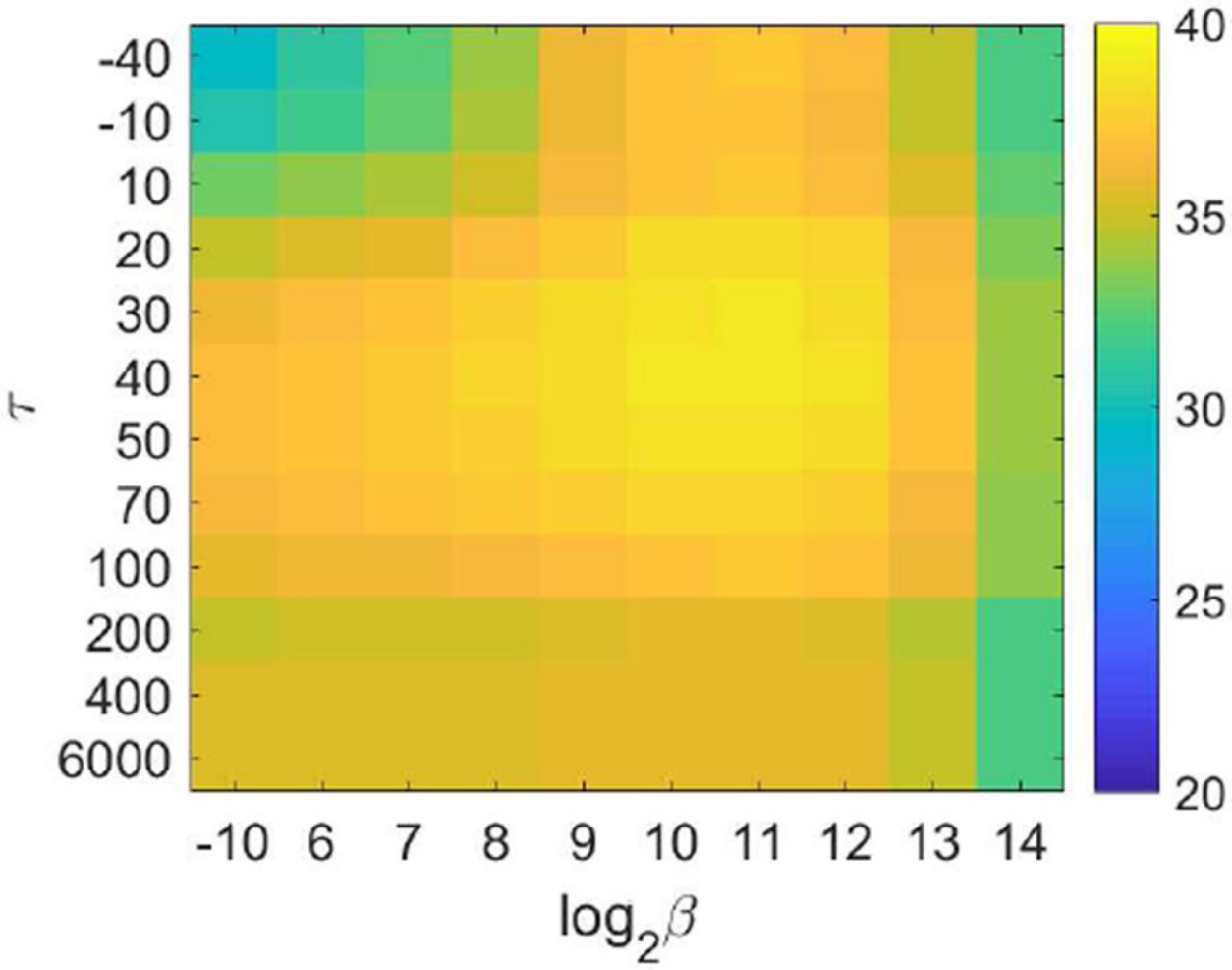

Fig. 10.
Combined effect of β and τ on image SNR of the hybrid reconstruction for the physical phantom data.

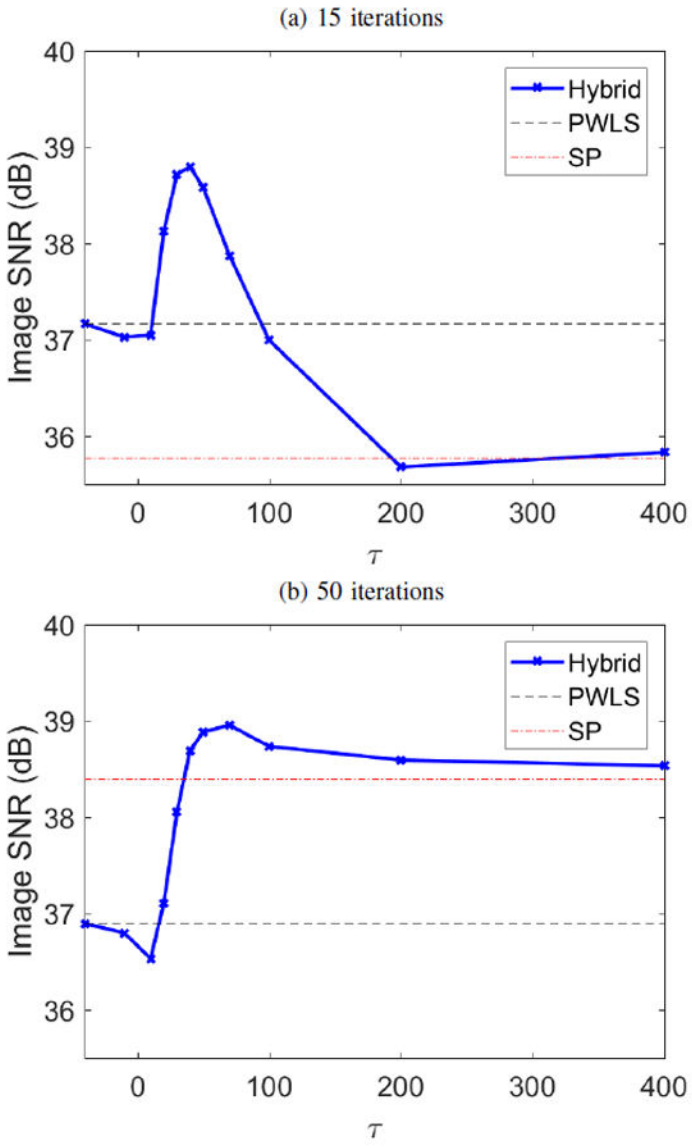

Fig. 11.

Effect of τ on image SNR of the hybrid reconstruction for the physical phantom data. $\beta = 2^{10}$.

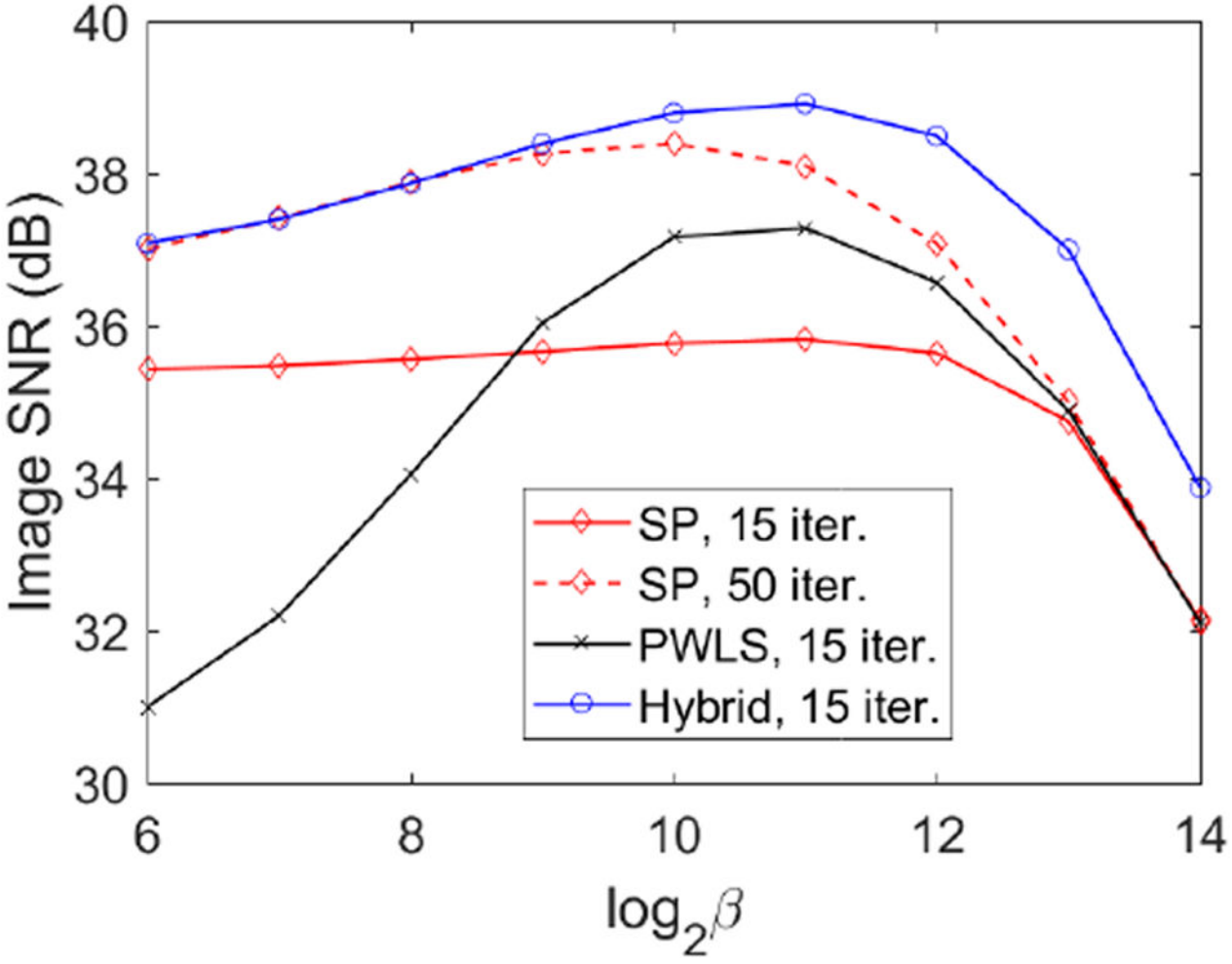

Fig. 12.

Effect of β on image SNR of three different methods for reconstructing the physical phantom data. The threshold parameter τ in the hybrid method is $\tau = 40$.